Geophysical Research Letters

RESEARCH LETTER
10.1029/2019GL082304

A Model for the Formation of Eskers

Ian J. Hewitt[1] and Timothy T. Creyts[2]

[1]Mathematical Institute, University of Oxford, Oxford, UK, [2]Lamont-Doherty Earth Observatory, Columbia University, Palisades, NY, USA

Key Points:
- We develop a quantitative physically based model for esker deposition in subglacial channels
- The model predicts relationships between melt rate, sediment supply, retreat rate, and esker size and spacing
- Larger ice sheet melt rates are expected to produce smaller, more closely spaced, eskers

Supporting Information:
- Supporting Information S1
- Text S1

Correspondence to:
I. J. Hewitt,
hewitt@maths.ox.ac.uk

Citation:
Hewitt, I. J., & Creyts, T. T. (2019). A model for the formation of eskers. *Geophysical Research Letters*, *46*, 6673–6680. https://doi.org/10.1029/2019GL082304

Received 31 JAN 2019
Accepted 21 MAY 2019
Accepted article online 29 MAY 2019
Published online 25 JUN 2019

Abstract We develop a mathematical model for esker formation by the continuous deposition of sediments near the mouth of water-filled subglacial tunnels. We assume a retreating ice sheet margin and prescribe meltwater and sediment supply to a channelized subglacial drainage system. The hydrodynamic model for the subglacial channel has its cross section governed by wall melting, creep closure, and sediment deposition. Sediment-carrying capacity typically increases downstream, before decreasing rapidly near the margin, suggesting that most deposition occurs there. This can lead to "choking" near the margin, which is offset by enhanced melting to keep the channel open. The model shows that the deposition rate varies roughly quadratically with sediment supply and inversely with water flux. For given sediment supply, the model suggests esker formation is most prevalent in smaller channels. Larger ice sheet melt rates likely produce more closely spaced eskers, but with smaller cross sections.

1. Introduction

Eskers are elongated ridges of sand and gravel that are widespread on the beds of the former Laurentide and Scandinavian Ice Sheets (Banerjee & McDonald, 1975; Brennand, 2000; Storrar et al., 2014a; Stroeven et al., 2016). Eskers are deposited in subglacial or ice-walled channels, and a quantitative understanding of the mechanisms underlying esker formation can provide insight into ice sheet drainage systems during past and future deglaciations (Clark & Walder, 1994; Livingstone et al., 2015; Shreve, 1985; Storrar et al., 2014b). The purpose of this paper is to provide a theoretical model for esker formation by the continuous deposition of sediments near the mouth of water-filled subglacial tunnels. This is the most commonly discussed mechanism for esker formation in the literature, but there is not yet an established mathematical description of the process. Our aim is to provide a quantitative basis for discussing how the spacing and size of eskers relate to the ice sheet and climate conditions under which they were formed.

The basic mechanism we discuss is well known and has been illustrated in schematic form in many previous papers (e.g., Banerjee & McDonald, 1975; Benn & Evans, 2010; Brennand, 2000; Warren & Ashley, 1994; see also Figure 1). Pressurized subglacial tunnel flow carries sand and gravel, which is deposited near the margin under conditions of declining sediment-carrying capacity. Deposition can occur both within the subglacial tunnel and beyond the margin in a proglacial stream or lake, where it forms a sedimentary fan. Our focus is on subglacial deposition, and we consider the process as a continual one, so that the esker represents an integral of the deposition that occurs during the retreating passage of the ice sheet margin. This is often referred to as "time-transgressive" deposition.

We restrict our attention to the simplest case of "steady" deposition because this must form a stepping-stone to more complex models that include episodic deposition. In this context we note the recent study of Beaud et al. (2018), whose model includes similar ingredients to our own but concentrates on time-dependent evolution on shorter timescales. In developing our model we are motivated by large-scale mapping studies that have suggested links between esker distribution and ice sheet conditions at the time of formation (e.g., Stroeven et al., 2016; Storrar et al., 2014b, 2014a). Storrar et al. (2014b) found a preferred esker spacing of around 12 km, with evidence for closer spacing during periods of more rapid retreat and therefore increased meltwater. Livingstone et al. (2015) compared mapped eskers with large-scale model estimates of subglacial water routing and found that eskers predominantly occur in regions where modeled water flow is low.

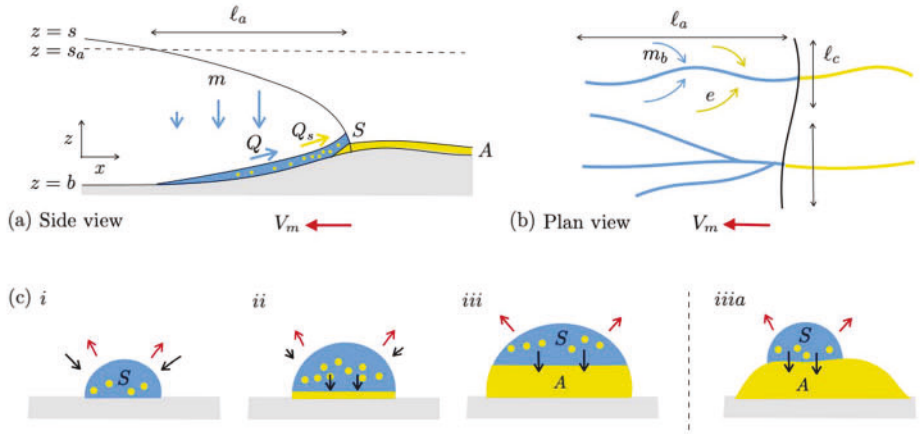

Figure 1. (a) Side and (b) plan views of the esker formation mechanism discussed in this paper. As the ice sheet margin retreats, subglacial channels of cross-sectional area S deposit sediments near the margin, leaving behind an esker of cross-sectional area A. The size of the deposit depends on sediment supply e, meltwater supply $m + m_b$, channel spacing ℓ_c, and retreat rate V_m, all of which can vary through time. (c) Downstream evolution of channel cross section. Red arrows denote wall melting. Black arrows denote creep closure and sediment deposition. (i) Far from the margin sediment flux is below the carrying capacity and the cross-sectional area S is governed by a balance between wall melting and creep closure; (ii) as the margin is approached and the channel enlarges, deposition starts to occur; (iii) at the margin a deposit of cross-sectional area A is formed and there is a balance between wall melting and deposition; (iiia) alternatively, the channel may move from side to side over time, depositing sediment over a wider area (the model does not distinguish between the situations in (iii) and (iiia)).

2. Mathematical Model

The model is primarily concerned with a single subglacial tunnel, beneath a steadily retreating ice sheet margin. More details and discussion of the assumptions behind this model are provided in the supplementary material. A schematic illustration is shown in Figure 1. The tunnel drains a catchment of width ℓ_c and length ℓ_a. It is fed by basal meltwater m_b and surface meltwater m from the ice sheet surface. The timescales of interest are large, so the seasonal cycle is ignored; these rates are best treated as maximum summer values since we expect that is when most sediment transport and deposition occurs. There is a basal sediment supply e from the surrounding bed, which we assume to be prescribed. Integrating over the catchment width, mass conservation determines the channel water flux Q and sediment flux Q_s from

$$\frac{\partial Q}{\partial x} = \ell_c(m_b + m), \tag{1}$$

$$\frac{\partial Q_s}{\partial x} = \ell_c e - D, \tag{2}$$

where x is distance along the channel and D is the sediment deposition rate (see below). This also controls the cross-sectional area of the deposited sediment A, according to

$$\frac{\partial A}{\partial t} = \frac{D}{1 - n_s}, \tag{3}$$

where n_s is the porosity of the deposited sediments. The combination (2) and (3) can equivalently be expressed as an Exner equation, by eliminating D.

The standard Röthlisberger theory for a subglacial tunnel has the cross-sectional area S evolving due to ice wall melting and creep closure (Figure 1c [i]). Deposition acts as an additional mechanism to reduce the size of the tunnel (Figure 1c [ii–iii]), so the equation governing cross-sectional area evolution is (Beaud et al., 2016; Creyts et al., 2013)

$$\frac{\partial S}{\partial t} = \frac{Q(\Psi - \beta\rho_w g b_x)}{\rho_i(1 + \beta)L} - \frac{2A_{\text{Glen}}}{n^n} S N^n - \frac{D}{1 - n_s}. \tag{4}$$

The first term here represents wall melting: Q is the water flux, Ψ is the hydraulic potential gradient, ρ_i is the ice density, L is the latent heat, $\beta = \rho_w c_w \gamma/(1 - \rho_w c_w \gamma)$ is a term that accounts for the pressure dependence

of the melting point, and b_x is the bed slope (positive for upslope in the direction of water flow). The second term represents creep closure: N is the effective pressure and A_{Glen} and n are the coefficients in Glen's flow law (Cuffey & Paterson, 2010). The hydraulic potential gradient is given by $\Psi = -\rho_i g s_x - (\rho_w - \rho_i) g b_x + N_x$, where s is the surface elevation and b the bed elevation.

The sediment flux and deposition rate are together determined from (2) by the fact that the sediment flux Q_s cannot exceed a carrying capacity Q_{eq}, which is taken to be a function of water velocity (Q/S) and channel width. Either the sediment flux is below the carrying capacity, $Q_s < Q_{\text{eq}}$, in which case $D = 0$, and (2) relates the flux directly to sediment supply (supply-limited conditions); or the sediment flux is *at* the carrying capacity, $Q_s = Q_{eq}$, in which case (2) serves to determine the deposition rate D (transport-limited conditions). Negative values of D correspond to erosion or remobilization of previously deposited sediment. The bed of the channel itself is not erodible (all sediment is assumed to be supplied by the prescribed source e) but negative values of D are allowed if there is a preexisting deposit A that can be remobilized.

Based upon the form of the Meyer-Peter Müller transport relation (Meyer-Peter & Mueller, 1948), which suggests $Q_{eq} \propto (\tau^* - \tau_c^*)^{3/2}$ where τ^* is the Shields stress, and accounting for the width $\propto S^{1/2}$ of the semicircular cross section, we adopt the following expression for the carrying capacity (see supporting information),

$$Q_{eq}(Q,S) = 8\left(\frac{8\Delta\rho_s g d^3 S}{\pi\rho_w}\right)^{1/2} \max\left(\frac{f\rho_w Q^2}{\Delta\rho_s g d S^2} - \tau_c^*, 0\right)^{3/2}. \quad (5)$$

Here τ_c^* is a critical Shields stress required for sediment mobilization, ρ_w is the density of water, $\Delta\rho_s = \rho_s - \rho_w$ is the buoyant density of sediment in water, g is the gravitational acceleration, d is a representative grain size, and f is a friction factor. The specific form of this law is not crucial to the theory, but simply that it increases with Q and decreases with S. Other formulations of sediment transport could be expressed in a similar form (e.g., Garcia & Parker, 1991; van Rijn, 1984).

Finally, the water flux is related to the tunnel's cross-sectional area S by a parameterization of turbulent drag,

$$Q = K_c S^{5/4} \Psi^{1/2}, \quad (6)$$

where K_c is a constant and Ψ is the hydraulic potential gradient (Flowers, 2015).

To summarize, the model has S and A evolving according to (3) and (4), with Q and N together determined from (1) and (6), and Q_s and D determined from (2) and (5). The required inputs are the meltwater and sediment source terms, and the surface and bed topography. For the latter, we use surface and bed profiles calculated using a plastic ice approximation accounting for isostatic depression (Cuffey & Paterson, 2010), shown in Figure 2a. We consider solutions that are steady in a frame that retreats with the margin at speed V_m. Time derivatives are therefore replaced by advective terms ($-V_m \partial/\partial x$) in the frame of the retreating margin; the resulting term in (4) is very small and can be neglected, while that in (3) controls esker size as described below.

For our example solutions, the surface meltwater input is taken to be $m = \max(0, \lambda(s_a - s))$, where λ accounts for the decrease in melting with surface elevation (analogous to a lapse rate) and s_a is the elevation above which no melting occurs. Varying s_a is treated as a proxy for changing the climate. We also suppose (for want of an obvious better alternative) that the channel sediment source e is proportional to the melt supply m.

3. Results and Discussion

3.1. Summary of Model Results

Two example solutions to the model are shown in Figure 2 for different values of sediment input. We find that the sediment flux is typically supply limited over most of the channel's length, with deposition happening over a relatively short zone near the margin, where the carrying capacity drops (panel d). This is due to the reduced confining pressure there, which results in a larger channel, smaller potential gradient and hence lower fluid velocities. The same behavior was found in a slightly different model by Beaud et al. (2018). The choking effect of deposition slightly compensates for the reduced rate of creep closure, and results in increased wall melting compared to an equivalent channel with no sediment. This increased wall melting helps keep the channel open while sediment is continually deposited beneath it, allowing a large esker to build up over time.

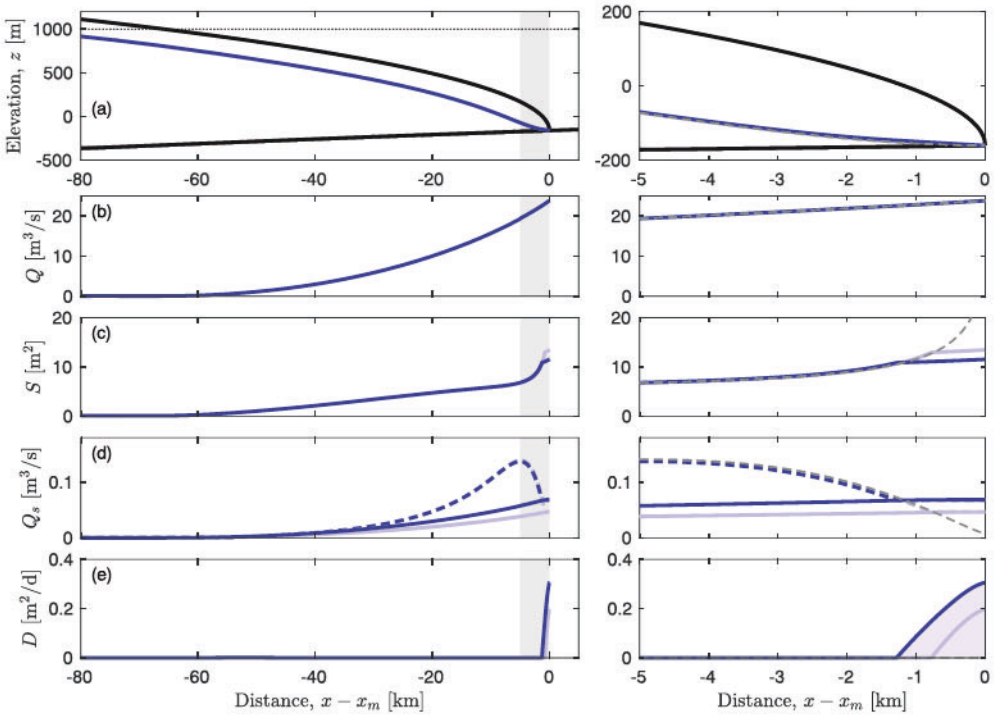

Figure 2. Steady solutions to the model showing (a) hydraulic head, (b) discharge, (c) cross-sectional area, (d) sediment flux (dashed line is carrying capacity Q_{eq}), and (e) deposition rate. Right-hand panels show an enlargement of the region near the margin. The sediment source e is proportional to the meltwater source, with $e/m = 0.003$ (darker shading) and 0.002 (lighter shading, obscured for most variables), and gray dashed lines show the equivalent solution when there is no sediment. Catchment width is $\ell_c = 10$ km, and the basal melt rate is $m_b = 5$ mm/year. Surface melt input is $m = \max(0, \lambda(s_a - s))$, where $\lambda = 3 \times 10^{-3}$ year^{-1} and $s_a = 1,000$ m is the elevation below which runoff starts, indicated by the dotted line in (a). The topography is also shown in black in (a). Other parameter values are in Table 1.

To determine the size of the deposited esker, we calculate the total (volumetric) deposition rate Q_D, which is the integral of D over the length of the deposition region and has units cubic meters per second (the shaded area under the curve in panel e). Integrating (3) over the period of margin retreat, we see that this is related to the cross-sectional area of the final deposit by the expression

$$A = Q_D/(1 - n_s)V_m. \tag{7}$$

This simply reflects that the size of the final deposit is determined by the total deposition rate and the amount of time that deposition has been occurring at each fixed location. Note that the solutions in Figure 2 and the resulting deposition rate do not themselves depend on the retreat rate, which affects esker size only through (7).

Due to the coupled dynamics of sediment and channel evolution, it is not at all obvious how the total deposition rate depends on inputs such as the melt rate, sediment supply, and spacing and length of channels, all of which may vary as the climate varies. To address this, we produce an ensemble of numerical solutions similar to Figure 2 and calculate the total deposition rate Q_D for each one. The result is shown in Figure 3a. Each solution has randomly chosen values for (i) the height s_a above which no melting occurs, (ii) the catchment width ℓ_c, and (iii) the ratio e/m of sediment supply to meltwater supply. These take values in the range [400–1,200] m, [2–20] km, and [0–0.003], respectively, and give a wide spectrum of deposition rates over several orders of magnitude.

Since deposition is mostly confined to the short region near the margin, we can characterize the influence of all the inputs in terms of the meltwater flux and the sediment flux that are delivered toward the margin, which are obtained from the integrals of (1) and (2). We write these "margin" values (with subscript m) as

$$Q_m = \ell_c M, \qquad Q_{sm} = \min\left(\ell_c E, Q_{s\,\max}\right), \tag{8}$$

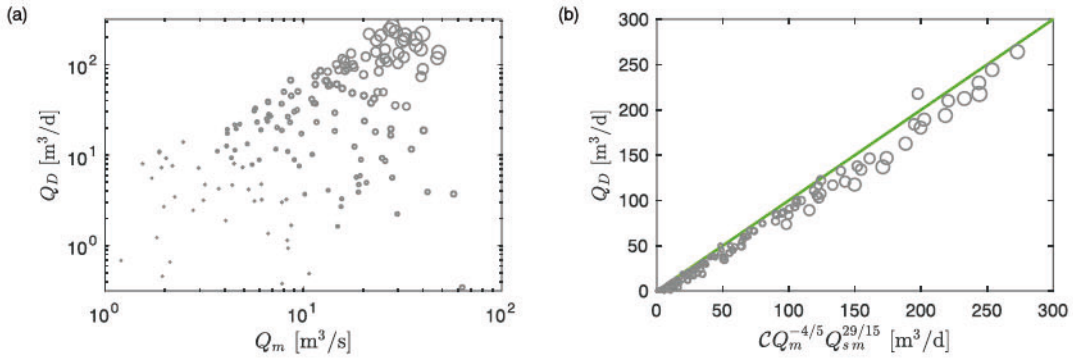

Figure 3. (a) Total deposition rate Q_D for an ensemble of 200 model solutions as described in the text, plotted as a function of the channel discharge at the margin Q_m, with size of the markers corresponding to the sediment flux at the margin Q_{sm}. (b) The same solutions plotted with the scaling (9), showing an approximate collapse.

where M is the total melt rate per unit width of the margin (integrated over the length of the channel ℓ_a) and E is the total sediment source per unit width of the margin. The cap $Q_{s\,\max}$ is the maximum carrying capacity of the channel (the peak of the dashed line in Figure 2d), which we find depends on the water flux according to $Q_{s\,\max} \approx 0.007\,Q_m^{21/22}$ (see supporting information). This cap accounts for the (unlikely) possibility of the upstream sediment flux being transport limited rather than supply limited.

By analyzing the behavior of the model in the relatively short deposition region near the margin, we find an approximate expression relating the total deposition rate Q_D to the margin discharge Q_m and sediment flux Q_{sm} defined in (8). This calculation is rather involved, so the details are left to the supporting information. The only important part of the calculation is the result

$$Q_D \approx C\,Q_m^{-4/5}\,Q_{sm}^{29/15}, \tag{9}$$

where $C \approx 5.6 \quad \mathrm{s}^{2/15} \quad \mathrm{m}^{-2/5}$ is a constant and where Q_{sm} and Q_m are expressed in cubic meters per second.

Table 1
Parameter Values

Parameter	Value
ρ_w	1,000 kg/m^3
ρ_i	916 kg/m^3
ρ_s	2,600 kg/m^3
g	9.8 m/s^2
L	3.3×10^5 J/kg
c_w	4,200 J·kg^{-1} ·K^{-1}
γ	7.5×10^{-8} K/Pa
n	3
A_{Glen}	2.4×10^{-24} Pa/s^3
K_c	0.11 m$^{3/2}$ kg$^{-1/2}$
d	1 mm
f	0.02
τ_c^*	0.047
n_s	0.3
β	0.46

Note. In addition, we take $\lambda = 3 \times 10^{-3}$ year^{-1} based on estimates of summer melting in Greenland, and $m_b = 5$ mm/year based on a geothermal energy balance.

We replot the numerical results in Figure 3b to demonstrate that the scaling in (9) does indeed provide a good approximation for the total deposition rate over a wide range of conditions. The expression in (9) is not exact, since it derives from an asymptotic approximation of a complicated model, but it does capture most of the dependence of Q_D on the input parameters. The strange exponents are due to a combination of nonlinearities in the sediment transport law, the parameterization of turbulent flow, and the flow law for ice. The precise values should be taken with a pinch of salt, since they change if a different parameterization is used for turbulent drag or for sediment flux. However, the fact that this deposition rate depends roughly quadratically on Q_{sm} and inversely on Q_m is quite robust.

The deposition rate Q_D combines with the retreat rate of the margin to determine the size of the esker in (7). For example, if water flux is 10 m^3/s, and sediment flux is 10^{-3} m^3/s (corresponding to around 2.6×10^{-3} t/s), the deposition rate is around 120 m^3/year. For a retreat rate of 10 m/year, the esker cross section is around 12 m^2. For a sediment flux 10 times larger, the esker would be almost 100 times larger. Note that for a given sediment supply, larger channels exhibit less deposition. This is because the larger channels maintain a larger water velocity near the margin, so are able to carry more of the sediment out to the proglacial environment.

3.2. Dependence on Climate and Sediment Supply

We now make use of the results above to suggest how changing climatic conditions may affect the deposition of eskers. To do this, we must consider how

the channel spacing and fluxes change with melt rate. We adapt scaling arguments given previously by Boulton et al. (2009), Schoof (2010), and Hewitt (2011). These are slightly different but all essentially boil down to establishing the distance over which water can be drawn laterally into a channel by the pressure difference between the channel and interchannel watershed. Treating the interchannel region of the subglacial system as a porous layer with transmissivity T, we find that major channel spacing, and hence esker spacing, are expected to scale as

$$\ell_c \sim \mathcal{B} M^{-19/87}. \tag{10}$$

where $\mathcal{B} \propto T^{15/29}$ is a constant derived in the supporting information and M is the melt rate introduced in (8). The transmissivity is highly uncertain and may have varied significantly depending on the nature of the distributed drainage system (e.g., permeable sediments vs. linked cavities; Boulton et al., 2009; Hewitt, 2011). A range of values $T = 10^4$–10^8 m^2/year together with parameters from Table 1, give $\mathcal{B} \approx$ 30–3,000 m$^{125/87}$s$^{-19/87}$, and for a typical value of $M = 10^{-3}$ m^2/s this gives a large range of estimates, $\ell_c \approx$ 0.1–14km. Observed esker spacing suggests that the larger end of this range may be more appropriate (Storrar et al., 2014a), assuming that eskers form in all the major drainage channels.

Based upon (10), we expect channel spacing to decrease with increasing overall melt rate M. An immediate implication is that eskers should be more closely spaced during times of increased runoff, which agrees with earlier work (Boulton et al., 2009; Hewitt, 2011; Storrar et al., 2014b). Coupled with the larger melt rate and expanded length of the catchment basins, the individual channel fluxes Q_m are still expected to become larger.

How the sediment flux Q_{sm} varies with melt rate is less clear. If the sediment supply were abundant, we might suppose that the sediment flux always attains its transport-limited maximum $Q_{s\,\max}$. However, the maximum carrying capacity is typically large, and given the need to sustain this with the sediment supply into the channel (e), we consider it more likely that the upstream sediment flux is supply limited (so $Q_{sm} = \ell_c E$ in (8), as is the case in our computations). For example, with a water flux of $Q = 100$ m^3/s (corresponding to an average melt rate of 6 m/year over a catchment of length 50 km and width 10 km), the maximum carrying capacity is $Q_{s\,\max} \approx 0.6$ m^3/s, or 1.5 t/s. This is around ten times higher than the average sediment flux found at a Greenland outlet stream (Cowton et al., 2012), and for a typical catchment of length 50 km and width 10 km, it would correspond to an average supply rate of 4 cm/year. Although this may be possible under transient conditions, it is likely that, on average at least, the sediment flux is less than the maximum carrying capacity.

If we instead suppose that the sediment supply E is constant, we expect the sediment flux Q_{sm} in each channel would decrease slightly with increasing melt rate due to the decrease in channel spacing. Moreover, even for constant sediment flux, the deposition rate Q_D decreases with increasing water flux, due to the more powerful stream flow carrying the sediment out past the margin. The model therefore suggests that there will be considerably less deposition, and therefore smaller eskers, when melt rate is higher. During rapid retreat of the margin this may be compounded by the reduced time for deposition at each location (7). This is consistent with the work of Livingstone et al. (2015), who found fewer eskers in regions where ice sheet models of past conditions suggest higher water flow.

3.3. Limitations and Extensions

The major simplification of this model is to treat channel dynamics as steady. On the timescale of margin retreat, it must be some long-term average behavior that controls esker deposition, but it is not obvious that can be described by the quasi-steady theory developed here. Channel size evolves on a timescale of days to weeks, so it could apply roughly to summer conditions, but short-term fluctuations are known to lead to more complicated dynamics (Beaud et al., 2018). We believe that the predicted scalings for deposition rate with melt rate and sediment supply are nevertheless useful, if only to provide a comparison for time-dependent models in the future.

Another significant limitation of our model is that we prescribe the sediment supply e. This is really controlled by a combination of erosion and the transport capacity of the distributed system that delivers it into the channel (possibly through periodic flushing by water flow in and out of the channel). We have also assumed a single grain size (sand) that is easily mobilized, and our results may not apply to much larger sediments such as boulders. A more detailed consideration of different sediment sizes would allow for greater

comparison with existing geological studies of eskers (e.g., Burke et al., 2015; Cummings et al., 2011), but this is beyond the scope of the current model.

One extension that can be considered is the role of bed topography, which was neglected in deriving (9). Shreve (1985) has shown that this has a significant effect on eskers, which tend to cross topographic saddle points and are lower and broader on an upsloping bed. This is believed to be due to the pressure dependence of the melting point; if the bed slopes upward in the direction of water flow, more of the heat generated from viscous dissipation is needed to keep the water at the melting point and less is therefore available for wall melting. In the supporting information, we examine how varying the bed slope b_x affects the deposition rate in our model. Deposition is reduced when the bed slope is positive (upward in the direction of flow) and is increased when it is negative. The surface slope in our model is set by the plastic ice approximation, but Beaud et al. (2018) found that surface slope also has a significant effect on deposition. It is therefore possible that the expression in (9) is not appropriate in all cases.

4. Conclusions

We have presented a mathematical description of water and sediment flow through subglacial channels that gives rise to esker deposition beneath a retreating ice margin. For a given channel water flux, the deposition rate varies with roughly the square of the sediment supply. For a given sediment supply, the deposition rate decreases roughly inversely with increasing water flux. The model further suggests that as ice sheet melt rates increase, eskers become more closely spaced but are smaller in cross section. The margin retreat rate also affects the size of the deposits, with smaller eskers expected where the margin retreats more rapidly. Larger esker sections are predicted where the margin is temporarily stable. Bed topography also plays a role, with smaller eskers predicted, or perhaps none at all, where the bed slopes significantly upward.

There remain many aspects of the dynamics that could be explored in future. In particular, the model could be solved in a time-dependent fashion, allowing for episodic deposition, and possible remobilization of esker material. The dynamics of a single channel explored here could also be built into a more complex model of two-dimensional channel networks, which would allow exploration of the role of tributaries and esker branching. Finally, we hope that the model predictions for deposition rate may aid in interpreting large-scale mapping studies of eskers.

Acknowledgments
I. J. H. was supported by a Marie Curie FP7 Career Integration Grant PCIG13-GA-2013-618007. T. T. C. was supported by the Vetlesen Foundation, U.S. Polar Programs Grant NSF-1643970, and NASA Cryosphere Grant NNX16AJ95G. No new data were used in this manuscript; all data can be found in cited references.

References

Banerjee, I., & McDonald, B. (1975). Nature of esker sedimentation. In A. Jopling, & B. McDonald (Eds.), *Glaciofluvial and glaciolacustrine sedimentation* (Vol. 23, pp. 132–154). Oklahoma: SEPM.

Beaud, F., Flowers, G. E., & Venditti, J. G. (2016). Efficacy of bedrock erosion by subglacial water flow. *Earth Surface Dynamics*, *4*(1), 125–145.

Beaud, F., Flowers, G., & Venditti, J. (2018). Modeling sediment transport in ice-walled subglacial channels and its implications for esker formation and proglacial sediment yields. *Journal of Geophysical Research: Earth Surface*, *123*, 3206–3227. https://doi.org/10.1029/2018JF004779

Benn, D., & Evans, D. J. (2010). *Glaciers and glaciation*. London: Hodder Education.

Boulton, G. S., Hagdorn, M., Maillot, P. B., & Zatsepin, S. (2009). Drainage beneath ice sheets: Groundwater-channel coupling, and the origin of esker systems from former ice sheets. *Quaternary Science Reviews*, *28*(7), 621–638.

Brennand, T. A. (2000). Deglacial meltwater drainage and glaciodynamics: Inferences from Laurentide eskers, Canada. *Geomorphology*, *32*, 263–293.

Burke, M. J., Brennand, T. A., & Sjogren, D. B. (2015). The role of sediment supply in esker formation and ice tunnel evolution. *Quaternary Science Reviews*, *150*, 50–77. https://doi.org/10.1016/j.quascirev.2015.02.017

Clark, P. U., & Walder, J. S. (1994). Subglacial drainage, eskers, and deforming beds beneath the Laurentide and Eurasian ice sheets. *Geological Society of America Bulletin*, *106*, 304–314.

Cowton, T., Nienow, P., Bartholomew, I., Sole, A., & Mair, D. (2012). Rapid erosion beneath the Greenland ice sheet. *Geology*, *40*, 343–346. https://doi.org/10.1130/G32687.1

Creyts, T. T., Clarke, G. K. C., & Church, M. (2013). Evolution of subglacial overdeepenings in response to sediment redistribution and glaciohydraulic supercooling. *Journal of Geophysical Research: Earth Surface*, *118*, 423–446. https://doi.org/10.1002/jgrf.20033

Cuffey, K., & Paterson, W. S. B. (2010). *The physics of glaciers*. Amsterdam: Academic Press.

Cummings, D. I., Gorrell, G., Guilbault, J.-P., Hunter, J. A., Logan, C., Ponomarenko, D., et al. (2011). Sequence stratigraphy of a glaciated basin fill, with a focus on esker sedimentation. *GSA Bulletin*, *123*, 1478–1496.

Flowers, G. E. (2015). Modelling water flow under glaciers and ice sheets. *Proceedings of the Royal Society A: Mathematical, Physical and Engineering Sciences*, *471*(2176), 20140907.

Garcia, M., & Parker, G. (1991). Entrainment of bed sediment into suspension. *Journal of Hydraulic Engineering*, *117*(4), 414–435.

Hewitt, I. J. (2011). Modelling distributed and channelized subglacial drainage: The spacing of channels. *Journal of Glaciology*, *57*, 302–314.

Livingstone, S., Storrar, R., Hillier, J., Stokes, C., Clark, C., & Tarasov, L. (2015). An ice-sheet scale comparison of eskers with modelled subglacial drainage routes. *Geomorphology*, *246*, 104–112.

Meyer-Peter, E., & Mueller, R. (1948). Formulas for bed load transport. In *Proceedings of 2nd meeting of the International Association for Hydraulic Structures Research, Delft, 7 June 1948*, pp. 39–64.
Schoof, C. (2010). Ice-sheet acceleration driven by melt supply variability. *Nature*, *468*, 803–806.
Shreve, R. L. (1985). Ekser characteristics in terms of glacier physics, Katahdin esker system, Maine. *Geological Society of America Bulletin*, *96*, 639–646.
Storrar, R. D., Stokes, C. R., & Evans, D. J. A. (2014a). Increased channelization of subglacial drainage during deglaciation of the Laurentide Ice Sheet. *Geology*, *42*, 239–242. https://doi.org/10.1130/G35092.1
Storrar, R. D., Stokes, C. R., & Evans, D. J. A. (2014b). Morphometry and pattern of a large sample (>20,000) of Canadian eskers and implications for subglacial drainage beneath ice sheets. *Quaternary Science Reviews*, *105*, 1–25. https://doi.org/10.1016/j.quascirev.2014.09.013
Stroeven, A. P., Hättestrand, C., Kleman, J., Heyman, J., Fabel, D., Fredin, O., et al. (2016). Deglaciation of Fennoscandia. *Quaternary Science Reviews*, *147*, 91–121.
van Rijn, L. C. (1984). Sediment transport, Part I: Bed load transport. *Journal of Hydraulic Engineering*, *110*, 1431–1456.
Warren, W. P., & Ashley, G. M. (1994). Origins of the ice-contact stratified ridges (eskers) of Ireland. *Journal of Sedimentary Research*, *A64*, 433–449.

References From the Supporting Information

Colgan, W., & Steffen, K. (2009). Modelling the spatial distribution of moulins near Jakobshavn, Greenland, *IOP Conference Series: Earth and Environmental Science* (Vol. 6, pp. 012022). Bristol, United Kingdom: IOP Publishing.
Einstein, H. A. (1968). Deposition of suspended particles in a gravel bed. *Journal of the Hydraulics Division Am Soc Civ Eng*, *94*, 1197–1205.
Hallet, B., Hunter, L., & Bogen, J. (1996). Rates of erosion and sediment evacuation by glaciers: A review of field data and their implications. *Global and Planetary Change*, *12*, 213–225.
Nye, J. (1952). A method of calculating the thickness of ice sheets. *Nature*, *169*, 529–530.
Nye, J. F. (1967). Plasticity solution for a glacier snout. *Journal of Glaciology*, *6*, 695–715.
Nye, J. F. (1976). Water flow in glaciers: Jökulhlaups, tunnels and veins. *Journal of Glaciology*, *17*, 181–207.
Phillips, B. C., & Sutherland, A. J. (1989). Spatial lag effects in bed load sediment transport. *Journal of Hydraulic Research*, *27*, 115–203.
Röthlisberger, H. (1972). Water pressure in intra- and subglacial channels. *Journal of Glaciology*, *11*, 177–203.
van Rijn, L. C. (1984b). Sediment Transport, Part II: Suspended load transport. *Journal of Hydraulic Engineering*, *110*, 1613–1641.
Weertman, J. (1961). Stability of ice-age ice sheets. *Journal of Geophysical Research*, *66*, 3783–3792.